Functional truncated membrane pores

Stoddart, David; Ayub, Mariam; Hoefler, Lajos; Raychaudhuri, Pinky; Klingelhoefer, Jochen W; Maglia, Giovanni; Heron, Andrew; Bayley, Hagan

Published in:
Proceedings of the National Academy of Science of the United States of America

DOI:
10.1073/pnas.1312976111

Functional truncated membrane pores

David Stoddart[1], Mariam Ayub, Lajos Höfler, Pinky Raychaudhuri, Jochen W. Klingelhoefer[2], Giovanni Maglia[3], Andrew Heron[1], and Hagan Bayley[4]

Department of Chemistry, University of Oxford, Oxford OX1 3TA, United Kingdom

Edited by Daniel Branton, Harvard University, Cambridge, MA, and approved January 2, 2014 (received for review July 10, 2013)

Membrane proteins are generally divided into two classes. Integral proteins span the lipid bilayer, and peripheral proteins are located at the membrane surface. Here, we provide evidence for membrane proteins of a third class that stabilize lipid pores, most probably as toroidal structures. We examined mutants of the staphylococcal α-hemolysin pore so severely truncated that the protein cannot span a bilayer. Nonetheless, the doughnut-like structures elicited well-defined transmembrane ionic currents by inducing pore formation in the underlying lipids. The formation of lipid pores, produced here by a structurally defined protein, is supported by the lipid and voltage dependences of pore formation, and by molecular dynamics simulations. We discuss the role of stabilized lipid pores in amyloid disease, the action of antimicrobial peptides, and the assembly of the membrane-attack complexes of the immune system.

alpha-hemolysin | beta-barrel | lipid reorganization | nanopore

Cells, and compartments within cells, are bounded by membranes, which are based on lipid bilayers. The overall width of a lipid bilayer from lipid head group to lipid head group is around 40 Å, with a hydrocarbon core that is about 30 Å across (1) (*SI Appendix*, Table S1). Proteins associated with membranes are usually divided into two classes. Integral proteins span the lipid bilayer, and peripheral proteins are located at the membrane surface, bound in many cases to integral proteins (2). Here we provide evidence for a third class of membrane proteins that stabilize lipid pores. These pores are most likely toroids, i.e., holes in the bilayer with a roughly circular cross-section and lined by lipid head groups. By contrast, integral membrane proteins are generally believed to span bilayers by displacing lipid molecules laterally rather than by reorganizing the bilayer structure. Toroidal lipid pores have been proposed previously in several contexts, for example for antimicrobial peptides (3, 4), but without a firm structural basis for the peptide or protein component.

We have explored mutants of the heptameric staphylococcal α-hemolysin (αHL) pore (5) in which the transmembrane β-barrel is so severely truncated that it cannot span a lipid bilayer (Fig. 1*A*). The barrel comprises 14 β-strands, two contributed by each of the seven subunits (5). Like the wild-type (WT) αHL pore, the truncated pores form conductive channels in lipid bilayers. The conductive pathway must traverse the center of the doughnut-like truncated structure and continue through the reorganized lipid bilayer. Further, the existence of these lipid pores is supported by the lipid and voltage dependences of pore formation, and by molecular dynamics simulations. Our observation of lipid pores induced by structurally defined proteins is of importance in several areas including amyloid disease (6, 7), the action of antimicrobial agents (8, 9), and the assembly of membrane-attack complexes of the immune system (10).

Results

Heptameric α-Hemolysin Pores with Truncated β-Barrels. Truncated barrel mutants (TBM) were made from the αHL NN mutant (Fig. 1*A*) (11) by pairwise removal of amino acids from both β-strands to yield barrels shortened by 2, 4, 6, 8, and 10 amino acids (Fig. 1 *B* and *C*). Although the full-length αHL NN monomer is stable in solution and assembles into heptamers only in the presence of rabbit erythrocyte membranes (rRBCm), the truncated αHL polypeptides assembled spontaneously during cell-free synthesis as judged by the formation of SDS-resistant oligomers (Fig. 1 *D* and *E*) that also resisted proteolysis (Fig. 1*F*). The latter properties are characteristic of the heptameric αHL pore containing full-length subunits. Native gel electrophoresis showed that TBMΔ2, Δ4, Δ6, and Δ8 formed structures with mobilities similar to the αHL NN heptamer, and TBMΔ10 formed a mixture of oligomeric structures. TBMΔ2 and Δ4 showed only weak hemolytic activity toward rabbit erythrocytes, and TBMΔ6, Δ8, and Δ10 were inactive (*SI Appendix*, Fig. S1), suggesting that the spontaneously formed heptamers cannot penetrate erythrocyte membranes, which is also the case for WT αHL heptamers (as opposed to WT monomers) (12).

Truncated α-Hemolysin Pores Conduct Ions Across Lipid Bilayers. TBMΔ2, Δ4, Δ6, and Δ8 pores were assembled in the presence of rRBCm, purified by SDS–polyacrylamide gel electrophoresis and examined by planar lipid bilayer recording (Fig. 2*A* and *SI Appendix*, Fig. S2). TBMΔ2 and Δ4 exhibited increased unitary conductance values compared with the full-length αHL NN pore, which would be expected for shortened pores based on the behavior of an electrolyte in a cylinder (13). By contrast, the unitary conductance values of TBMΔ6 and Δ8 were reduced, which is suggestive of a constricted or elongated conductive pathway (13). TBMΔ4 and Δ6 showed excess current noise by comparison with αHL NN (Fig. 2*A*), indicating conformational flexibility of these pores (*SI Appendix*, Table S2).

Significance

Cells and compartments within them are bounded by membranes, the underlying structure of which is the lipid bilayer. Molecules that move into and out of cells or between compartments are transported through protein channels and pores, which according to conventional thinking completely span the intact bilayer. However, indirect evidence has suggested the existence of a separate class of membrane proteins that perturb the bilayer structure to create transmembrane conduits. We present direct evidence for such proteins, and suggest that they are protagonists in important physiological processes, including defense by the immune system against microorganisms and neuronal damage in Alzheimer's disease.

Author contributions: D.S., M.A., L.H., P.R., G.M., A.H., and H.B. designed research; D.S., M.A., L.H., P.R., and J.W.K. performed research; D.S., M.A., L.H., P.R., and H.B. analyzed data; and D.S., M.A., L.H., and H.B. wrote the paper.

Conflict of interest statement: H.B. is the founder, a director, and a shareholder of Oxford Nanopore Technologies, a company engaged in the development of nanopore-sequencing technology. Work in the H.B. laboratory at the University of Oxford, including this work, is supported in part by Oxford Nanopore Technologies.

This article is a PNAS Direct Submission.

Freely available online through the PNAS open access option.

[1]Present address: Oxford Nanopore Technologies, Oxford OX4 4GA, United Kingdom.

[2]Present address: LabMinds, Oxford OX1 4HT, United Kingdom.

[3]Present address: Department of Chemistry, University of Leuven, 3001 Leuven, Belgium.

[4]To whom correspondence should be addressed. E-mail: hagan.bayley@chem.ox.ac.uk.

This article contains supporting information online at www.pnas.org/lookup/suppl/doi:10.1073/pnas.1312976111/-/DCSupplemental.

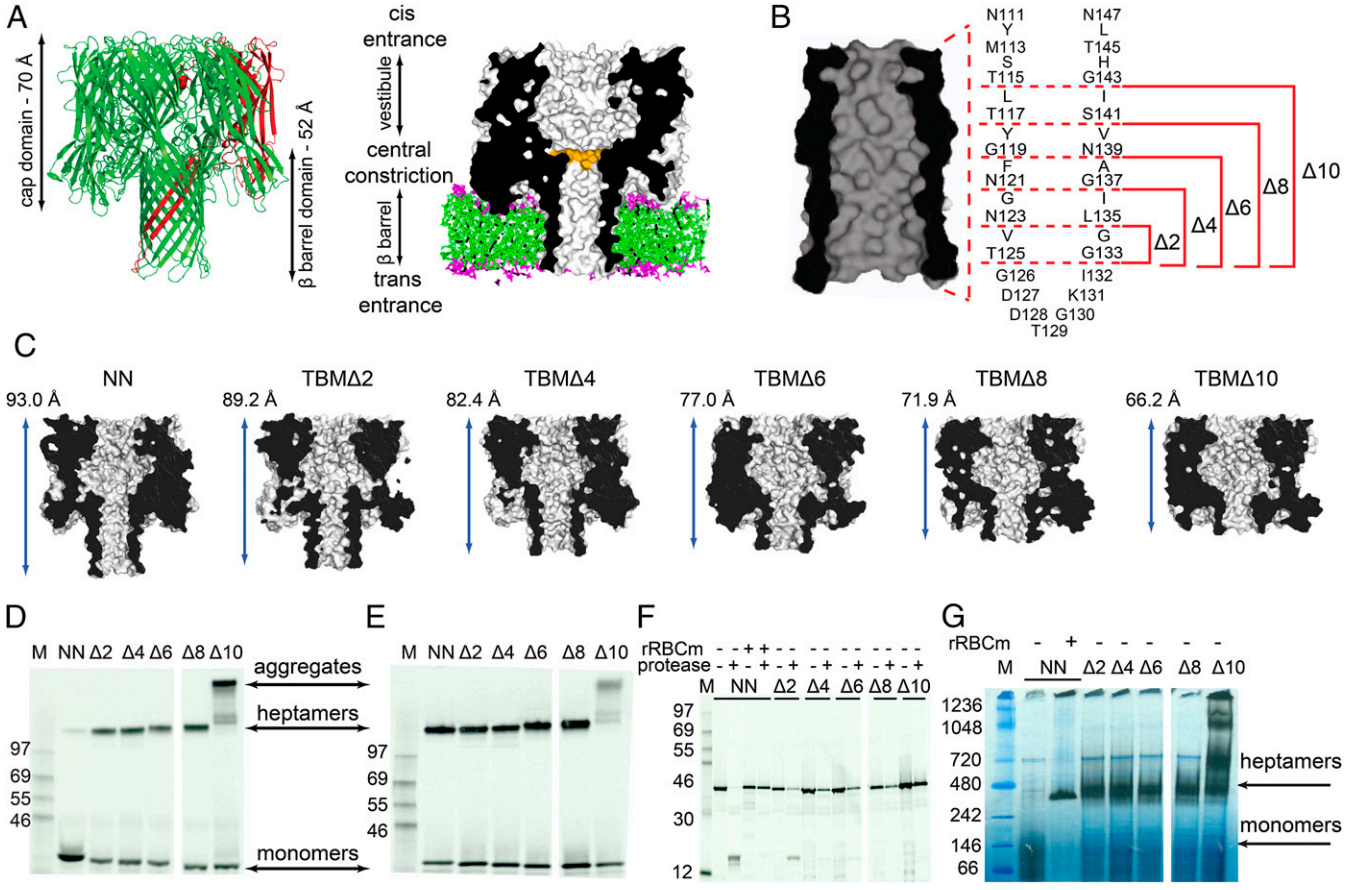

Fig. 1. Assembly of truncated αHL protein pores. (*A*) Cartoon (*Left*) and cut-through (*Right*) representations of the WT αHL pore (PDB ID code 7AHL). One subunit of the homoheptameric pore is colored red. The pore consists of an upper cap domain, which contains an approximately spherical, water-filled cavity or vestibule, and a transmembrane domain, which comprises a 14-stranded, antiparallel β-barrel. The TBM also contained the mutations E111N/K147N (NN), which remove charged residues (Glu and Lys) at the central constriction (orange, in cut-through). (*B*) Each of the seven subunits contributes two β-strands separated by a turn (residues 126–132) to the barrel. In the present study, 2, 4, 6, 8, or 10 consecutive residues were deleted from each of the two β-strands leaving the turn sequence intact. As a consequence, the TBM were altered by the removal of rings from the barrel, 2, 4, 6, 8, or 10 residues in height. (*C*) Cut-through representations of the TBM pores after homology modeling of the crystal structure of the αHL pore with MODELER and 10-ns all-atom molecular dynamics simulations. The length shown is the distance between the geometric center of the Cα atoms of amino acids Asn-17 from all seven subunits (located at the top of the cap domain) and the geometric center of the Cα atoms of amino acids Thr-129 from all seven subunits (located at the base of the transmembrane domain). (*D* and *E*) SDS/PAGE analysis of unheated samples after protein expression by in vitro transcription and translation in the absence (*D*) and presence (*E*) of rRBCm. In the case of *E*, a membrane pellet was analyzed. NN: full-length αHL E111N/K147N. (*F*) Limited proteolytic digests of freshly translated NN and TBM proteins with proteinase K. The full-length αHL NN protein was translated in the absence of rRBCm (-) and the presence of rRBCm (+). The samples were heat-denatured before SDS/PAGE. (*G*) Native PAGE analysis of the TBM proteins. The NN protein was translated in the presence and absence of rRBCm. The Coomassie blue stained gel, showing the molecular markers (M), is superimposed on an autoradiogram. In *F* and *G*, membrane pellets were analyzed in the +rRBCm lanes. In *D*–*G* the αHL polypeptides were labeled with [^{35}S]methionine. The molecular masses of the markers are in kDa.

TBMΔ8 was examined in more detail. When the lipid bilayer was formed from 100% 1,2-diphytanoyl-sn-glycero-3-phosphocholine (DPhPC), the TBMΔ8 pore opened and closed in bursts at +200 mV (Fig. 2*B*). The mean closed time was 13 ± 4 s, and the mean open time was 1.3 ± 0.3 s (n = 3 experiments, total of 490 events). By contrast, when the lipid was DPhPC containing 10% 1,2-dilauroyl-sn-glycero-3-phosphocholine (DLPC), the TBMΔ8 pore remained open almost continuously at +200 mV, with frequent spikes toward zero current (Fig. 2*C*). DLPC has shorter fatty acyl chains than DPhPC and the chains are unbranched (Fig. 2*C* and *SI Appendix*, Fig. S10). Therefore, this experiment suggests that the bilayer thins in the vicinity of the pore, possibly forming a toroidal lipid ring. The latter structure is favored by DLPC (Fig. 2*C*), which has a greater tendency than DPhPC to form micelles with curved surfaces (14, 15). The TBMΔ8 pore also closed at low applied membrane potentials (*SI Appendix*, Fig. S3), supporting the idea of a lipid toroid, which is favored at high potentials (16–18).

The Truncated Pores Bind Cyclodextrin Adapters. Cyclodextrins (CD) bind within the β-barrel of the WT αHL pore (19–21), and binding is sensitive to small perturbations in the structure of the pore (21) or the cyclodextrin itself (22). To test the integrity of the barrel in TBM mutants, we measured the association and dissociation rate constants of β-cyclodextrin (βCD), heptakis-(6-deoxy-6-amino)-β-cyclodextrin (am$_7$βCD) and γ-cyclodextrin (γCD) (*SI Appendix*, Figs. S4–S7). The binding of γCD showed a clear decrease in affinity (increase in K_D) as the pores became shorter. This is reasonable, because the bulky γCD may bind at the lower cyclodextrin site near residue 139 (20), rather than at the upper site near the central constriction (Fig. 1*A*; ref. 21). The effects of truncation on βCD and am$_7$βCD binding were less marked in the TBMΔ2 and TBMΔ4 pores, whereas the affinity for TBMΔ6 pore was significantly reduced. TBMΔ8 and TBMΔ10 do not bind the cyclodextrins. We display representative current traces showing the interaction of βCD, am$_7$βCD, and γCD with TBMΔ6 (Fig. 2*D*). It is interesting to note that although TBMΔ6 binds am$_7$βCD weakly

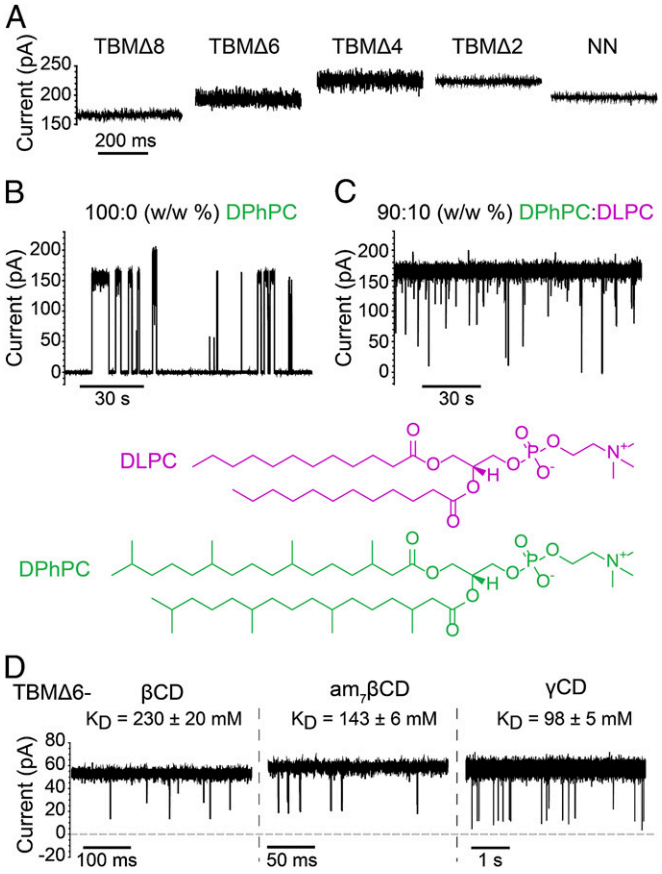

Fig. 2. Electrical recordings from truncated αHL pores. (*A*) Single-channel recordings of the αHL NN and TBMΔ2 to Δ8 pores. Purified proteins were incorporated into DPhPC bilayers in 1 M KCl, 25 mM Tris HCl, pH 8.0, with 0.1 mM EDTA. A potential of +200 mV was applied to the *trans* compartment with the *cis* compartment connected to ground. The current signals were filtered at 1 kHz and acquired at 5 kHz. Typical current traces in the open pore state are shown. (*B*) In 100% DPhPC bilayers, TBMΔ8 pores opened transiently at +200 mV in 1 M KCl, 25 mM Tris.HCl, pH8.0, with 0.1 mM EDTA. (*C*) The duration of the open state was considerably lengthened when the DPhPC bilayer was supplemented with 10% (wt/wt) DLPC, which has shorter, unbranched fatty acid chains, by comparison with DPhPC. (*D*) Representative current traces from TBMΔ6 showing transient blockades by βCD, am$_7$βCD and γCD. The current traces have been filtered (post acquisition) at 5 kHz, with a 4-pole Bessel filter, for presentation purposes. The dissociation constants ($K_D = k_{off}/k_{on}$) were calculated from the association (k_{on}) and dissociation (k_{off}) rate constants (*SI Appendix*, Figs. S4–S6). Kinetic data for cyclodextrin binding to the αHL NN pore, TBMΔ2 and TBMΔ4 were also obtained (*SI Appendix*, Fig. S7). Each recording ($n = 3$, for each TBM mutant and each cyclodextrin) lasted 5–15 min and included thousands of events.

(k_{off} = 4600 ± 300 s^{-1}, K_D = 151 ± 8 mM), the mutation Met-113→Phe, which strengthens βCD binding in the untruncated pore (21), dramatically improved am$_7$βCD binding to TBMΔ6. The am$_7$βCD remained bound to TBMΔ6/M113F for more than 1.5 h at potentials of +60 to +140 mV (*SI Appendix*, Fig. S11). In TBMΔ8, residues in the vicinity of Met-113 are presumably perturbed.

Molecular Dynamics Simulations Support the Formation of Lipid Pores. Coarse-grained molecular dynamics (MD) simulations were performed on TBMΔ6 and TBMΔ8 to better understand the effects of lipid composition on pore formation (23). The protein was placed in an equilibrated bilayer of 90 mol% 1,2-dipalmitoyl-sn-glycero-3-phosphocholine (DPPC) and 10 mol% DLPC (*SI Appendix*, Fig. S10). The lipid molecules under the remaining β-barrel and those in contact with the underside of the αHL cap domain were removed. At this point, the remaining lipid molecules were normal to the plane of the bilayer. The system was solvated and K^+ and Cl^- ions were added to give 0.5 M KCl. Seven additional Cl^- ions were added to neutralize the positive charge on the protein. Steepest decent energy minimization and 4 ns of preconditioning MD were run with a constant number of particles and at constant volume. At 0 ns after preconditioning, the protein sat in a thinned bilayer in which the *trans* opening of the truncated β-barrel was not occluded by lipids (Fig. 3*A*, *Left* and *SI Appendix*, Fig. S8*A*). In the case of TBMΔ6, after 400 ns, the bilayer assumed a largely toroidal character with the lipid head groups lining the bottom part of the conductive pathway. The radial distribution of the DLPC molecules was determined at 0, 400, 800, and 1,600 ns (Fig. 3*A* and *SI Appendix*, Fig. S8). The mole fraction of DLPC remained at ~10% at distances more than 4 nm from the central axis of the protein for the entire simulation (Fig. 3). However, after 800 ns, the mole

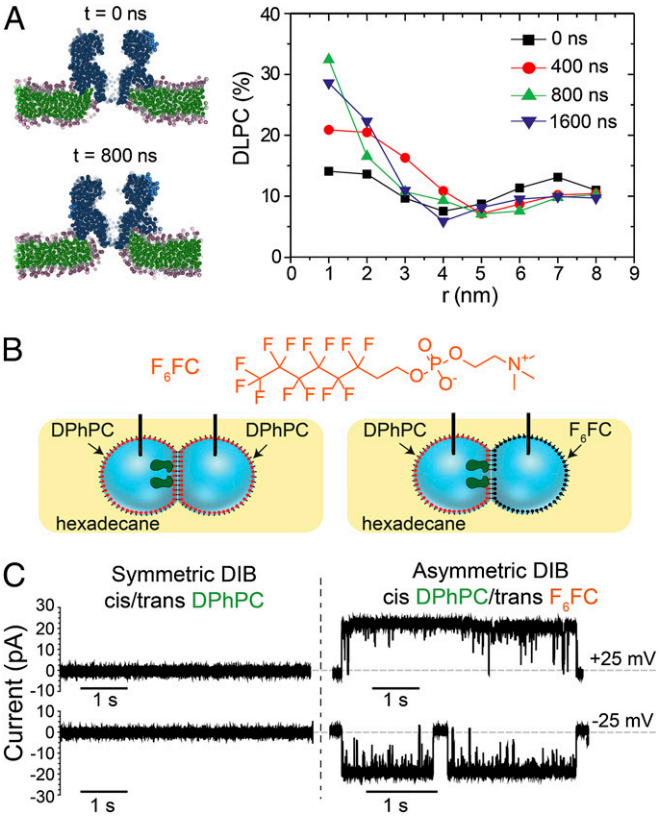

Fig. 3. Interactions with lipids. (*A*) Coarse-grained molecular dynamics simulations were performed on TBMΔ6 in a 90% DPPC/10% DLPC bilayer. The system was solvated in 0.5 M KCl. Seven additional Cl^- ions were added to neutralize the positive charge on the protein. (*Upper Left*) At 0 ns, after equilibration, the protein sits in a thinned bilayer. (*Lower Left*) At 800 ns, the bilayer has assumed a largely toroidal character with the lipid head groups lining the lower part of the conductive pathway. (*Right*) The mol% of DLPC in radial segments of the lipid bilayer was determined at 0, 400, 800, and 1,600 ns. Values are plotted versus the distance (*r*) from the central axis of the pore (*SI Appendix*, Fig. S9). (*B*) The interaction of TBMΔ8 with a bilayer containing one fluorinated leaflet. (*Upper*) Structure of [1H, 1H, 2H, 2H-perfluorooctyl) phosphocholine (F_6FC)]. (*Lower Left*) Schematic of DIB formed entirely from DPhPC. (*Lower Right*) DIB formed from DPhPC in one leaflet and F_6FC in the other. The vertical rods represent electrodes. (*C*, *Left*) Single-channel current traces at +25 and −25 mV of TBMΔ8 in a symmetrical DIB formed from DPhPC. (*Right*) Single-channel current traces at +25 and −25 mV of TBMΔ8 in an asymmetric DIB formed from one DPhPC leaflet and one F_6FC leaflet. TBMΔ8 was inserted from the DPhPC side. Typical traces are shown. The experiments were repeated ($n = 3$), yielding a total of 411 events (+25 mV) and 536 events (−25 mV). The current signals were filtered at 1 kHz and acquired at 10 kHz.

fraction of DLPC in the vicinity of TBMΔ6 rose to 30% (Fig. 3*A*), i.e., DLPC became concentrated in the toroid. TBMΔ8 showed reduced affinity for the lipid bilayer, and was extruded onto the bilayer surface (*SI Appendix*, Fig. S8*B*), consistent with the frequent closures observed for TBMΔ8 at low applied potentials (Fig. 2*B* and *SI Appendix*, Fig. S3). However, we cannot distinguish between various mechanisms for the opening and closing of the TBM pores in electrical recordings. Gating could be caused by the truncated end of the pore collapsing and reopening, or by pores leaving the bilayer, as seen in the MD simulations of TBMΔ8, and reinserting into it.

Short-Chain Fluorinated Amphiphiles Facilitate Pore Formation. The interaction of TBMΔ8 with bilayers containing one fluorinated leaflet was examined by using droplet interface bilayers (DIBs) (24). In DIBs formed from two DPhPC leaflets, TBMΔ8 behaved in much the same way as it did in conventional planar lipid bilayers of the same composition, producing pores with short-lived openings that closed at applied potentials below +100 mV (Fig. 3*B*). In asymmetric bilayers (25) with one leaflet of DPhPC and the other comprising the short single-chain fluorinated amphiphile fluorinated fos-choline (F_6FC; Fig. 3*B*), TBMΔ8 added from the DPhPC side of the bilayer formed long-lived pores, which stayed open at low applied potentials (±25 to ±100 mV): mean open times 2.2 ± 0.8 s (−25 mV), 6.4 ± 4.4 s (+25 mV); mean closed times 190 ± 40 ms (−25 mV), 46 ± 17 ms (+25 mV). TBMΔ8 inserted into the asymmetric bilayers from the DPhPC side far more readily than it inserted into symmetric DPhPC (i.e., at 25 times higher dilution). By contrast, TBMΔ8 inserted into the F_6FC side of the asymmetric bilayer only when it was applied at 50 times the concentration required for the DPhPC side, and in this case the pores that formed were short lived. In accord with the idea of a lipid toroid, the presence of the wedge-shaped F_6FC in the *trans* leaflet of the asymmetric bilayer facilitated pore opening and led to longer open times, by comparison with symmetrical bilayers with two DPhPC leaflets.

Discussion

Here, we have explored the functional properties of a series of truncation mutants of the heptameric staphylococcal αHL pore. Our results indicate that, except for the deleted residues, the truncated pores (TBMΔ2 to Δ8) have structures that are closely similar to that of the full-length heptameric αHL pore (5). The truncated pores are SDS and protease resistant indicating that they are correctly folded. They have mobilities in SDS and native gels that are similar to that of the full-length heptamer indicating that they too are heptamers. Additional evidence indicates that the internal structures of the truncated pores are similar to that of the full-length heptamer: TBMΔ2 to Δ6 bind cyclodextrins (in particular, the mutant TBMΔ6/M113F binds am$_7$βCD very tightly) and the unitary conductance values of the pores are in the same range as that of the full-length pore.

TBMΔ6 and TBMΔ8, which are missing a remarkable 12 and 16 amino acids per subunit, form pores in planar lipid bilayers. We suggest that an open TBM protein ring sits on the bilayer surface and stabilizes a lipid pore, most likely in the form of a toroidal defect. In keeping with the latter, the conductance values of TBMΔ6 and TBMΔ8 are lower than expected were the conductive pathway simply shortened. The experimental findings are supported by MD simulations. Transient pores have been observed in lipid bilayers in the absence of protein for over 30 y (16, 26, 27). These pores have been discussed extensively in terms of structural fluctuations (26, 27) and observed in MD simulations (28–30). For example, Antonov and colleagues found current fluctuations in bilayers of DSPC near the phase transition temperature (31).

As an alternative to lipid pore formation, the truncated αHL pores might adapt to and span lipid bilayers by one of the several mechanisms that have been proposed to accommodate "hydrophobic mismatches," all of which assume that the bilayer remains structurally intact (32–34). For shortened structures, these mechanisms include contraction of the acyl chains, and tilting, bending or aggregation of the inserted protein (33). Because the truncations we have made are extensive, they cannot be accommodated by contraction of the lipids. Alterations of the protein orientation or structure are viable mechanisms for α-helices, for which they were devised, but they do not work for β-barrels with large hydrophilic caps. The membrane protein with the thinnest structurally defined hydrophobic domain is the ClC chloride channel/transporter at 23 Å (32), but the associated lipid head groups have not been confirmed to be unusually closely spaced. All in all, lipid pore formation is the most likely option that is consistent with the functional properties of the αHL TBM mutants.

We have previously developed a prepore model for assembly of the αHL pore (35, 36), which has proved to be generally applicable to a range of pore-forming toxins including the β-barrel cholesterol-dependent cytolysins (37) and the α-helical pores

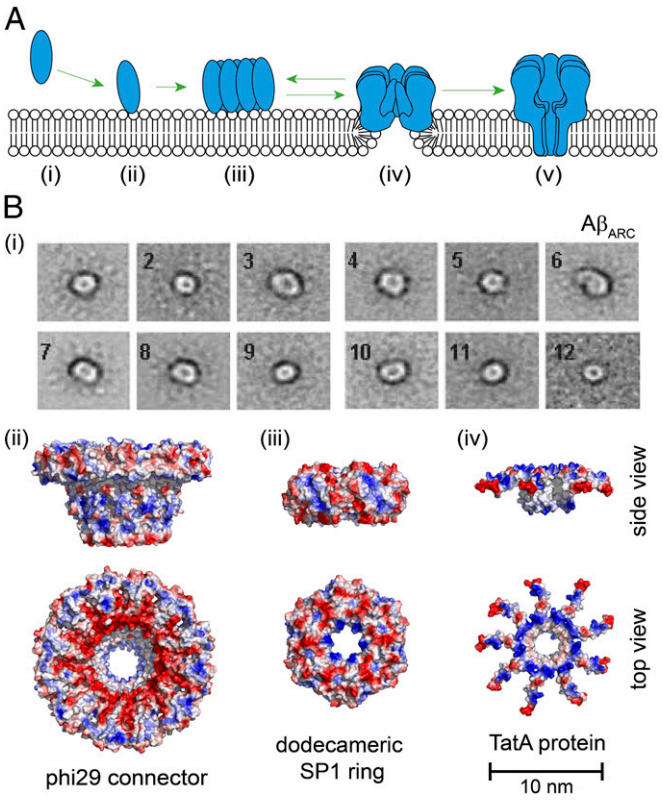

Fig. 4. Lipid pores in assembly intermediates and functional pores. (*A*) A revised model for the assembly of pore-forming toxins and related membrane proteins. (*i*) A monomeric toxin, such as αHL (depicted), binds to the bilayer surface (*ii*). This step may be receptor mediated (46). (*iii*) The membrane-bound monomer assembles (47) into an oligomeric prepore (35, 36), which does not penetrate the lipid bilayer. In the case of αHL, the prepore (and pore) is a heptamer. In some cases, prepore formation may occur in the bulk aqueous phase (48), before binding to the bilayer surface. (*iv*) The prepore induces lipid pore formation as described in the present paper. (*v*) The transmembrane β-barrel is formed when polypeptide sequences stored in the central cavity of the prepore descend into the aperture provided by the lipid pore. (*B*, *i*) Annular structures formed by a disease-associated mutant of amyloid-β (Aβ) (Artic variant E22G) visualized by electron microscopy (6). The outer diameters of the rings are 6–9 nm. (*ii*) The phi29 connector (PDB ID code 1FOU) (43). (*iii*) The dodecameric SP1 ring (PDB ID code 1TR0) (44). (*iv*) Ring formed by the TatA protein from the twin-arginine transport system (PDB ID code 2LZS) (45). Negatively charged residues are colored in red and positively charged residues in blue.

ClyA (38) and FraC (39). In the case of αHL, the prepore resembles the truncated heptameric structures of the present work, except that the cavity within the cap domain contains the polypeptide sequences that go on to form the membrane-spanning β-barrel. We now suggest an elaboration of the assembly model in which a transient lipid pore appears in the bilayer beneath the prepore structure. On the first opening of this pore, or perhaps during subsequent openings, the barrel-forming residues move into the aperture, and irreversible barrel formation occurs without the need to displace bilayer lipid (Fig. 4*A*).

Other pores might assemble through a similar pathway including the membrane-attack complexes and perforin pores of the immune system (10). However, other pore-forming proteins might stabilize lipid pores as the endpoint in their assembly, including the proteins involved in permeabilizing mitochondria during apoptosis (40, 41) and the membrane-active bacteriocins, such as colicin E1 (42). Peptide antimicrobial agents, such as magainins, have also been proposed to stabilize or line toroidal pores (3, 4, 8, 9). It is also possible that the annular amyloid protein aggregates that have been suggested to mimic bacterial pore-forming toxins (6, 7) operate through a lipid-pore mechanism (Fig. 4 *B*, *i*). Protein rings that permeabilize bilayers but do not have a hydrophobic surface may also function from on top of the bilayer, including the phi29 connector (43) (Fig. 4 *B, ii*) and the dodecameric SP1 (44) (Fig. 4 *B, iii*). Rings too thin to span a bilayer, such as the TatA protein from the twin-arginine transport system (45), may act in a similar way (Fig. 4 *B, iv*).

Materials and Methods

Protein Procedures. The αHL truncated barrel mutants were generated from the NN αHL gene (11) in a pT7 vector by PCR mutagenesis and ligation-free in vivo recombination. The αHL polypeptides were obtained by in vitro transcription and translation; the supernatant was used after centrifugation at 25,000 × *g*. Hemolytic assays were carried out by monitoring the decrease in light scattered at 595 nm with a microplate reader. Oligomeric structures formed by TBM and their sensitivity to SDS were examined with the NativePAGE gel system (Invitrogen, Ltd.). The products of limited proteolysis with proteinase K were analyzed with 12% SDS–polyacrylamide gels.

Electrical Recordings. Ionic current measurements were performed with a conventional planar bilayer apparatus, except for the study of fluorinated bilayers, which was carried out with droplet interface bilayers (24). Data were analyzed and prepared for presentation with pClamp (version 10.1, Molecular Devices). OriginPro8 was used for further analysis.

MD Simulations. Coarse-grained molecular dynamics simulations were performed by placing the TBMΔ6 and TBMΔ8 αHL pores in a simulation box of 18 × 18 × 18 nm initial dimensions, containing an equilibrated 90 mol% DPPC/10 mol% DLPC bilayer. K^+ and Cl^- ions were added to give a final concentration of 0.5 M KCl. The final system included ∼60,000 beads. Simulation analysis was carried out with GROMACS software with periodic boundary conditions at a constant temperature and pressure and with a 20-fs time step.

Full *Methods* and associated references are available in the *SI Appendix*.

ACKNOWLEDGMENTS. This work was supported by grants from the National Institutes of Health, the European Commission's Seventh Framework Programme (FP7) READNA Consortium, Oxford Nanopore Technologies, and a European Research Council Advanced Investigator award. D.S. was supported by a Biotechnology and Biological Sciences Research Council doctoral training grant, P.R. by a Felix Scholarship, and J.K. by the Engineering and Physical Sciences Research Council.

1. White SH, Ladokhin AS, Jayasinghe S, Hristova K (2001) How membranes shape protein structure. *J Biol Chem* 276(35):32395–32398.
2. White SH. Membrane proteins of known 3D structures, Stephen White Laboratory (UC Irvine). Available at http://blanco.biomol.uci.edu/mpstruc/. Accessed January 10, 2013.
3. Ludtke SJ, et al. (1996) Membrane pores induced by magainin. *Biochemistry* 35(43): 13723–13728.
4. Matsuzaki K, Murase O, Fujii N, Miyajima K (1996) An antimicrobial peptide, magainin 2, induced rapid flip-flop of phospholipids coupled with pore formation and peptide translocation. *Biochemistry* 35(35):11361–11368.
5. Song L, et al. (1996) Structure of staphylococcal alpha-hemolysin, a heptameric transmembrane pore. *Science* 274(5294):1859–1866.
6. Lashuel HA, Lansbury PT, Jr. (2006) Are amyloid diseases caused by protein aggregates that mimic bacterial pore-forming toxins? *Q Rev Biophys* 39(2):167–201.
7. Demuro A, Smith M, Parker I (2011) Single-channel Ca(2+) imaging implicates Aβ1-42 amyloid pores in Alzheimer's disease pathology. *J Cell Biol* 195(3):515–524.
8. Brogden KA (2005) Antimicrobial peptides: Pore formers or metabolic inhibitors in bacteria? *Nat Rev Microbiol* 3(3):238–250.
9. Cirac AD, et al. (2011) The molecular basis for antimicrobial activity of pore-forming cyclic peptides. *Biophys J* 100(10):2422–2431.
10. Rosado CJ, et al. (2008) The MACPF/CDC family of pore-forming toxins. *Cell Microbiol* 10(9):1765–1774.
11. Gu L-Q, et al. (2000) Reversal of charge selectivity in transmembrane protein pores by using noncovalent molecular adapters. *Proc Natl Acad Sci USA* 97(8):3959–3964.
12. Bhakdi S, Füssle R, Tranum-Jensen J (1981) Staphylococcal alpha-toxin: Oligomerization of hydrophilic monomers to form amphiphilic hexamers induced through contact with deoxycholate detergent micelles. *Proc Natl Acad Sci USA* 78(9):5475–5479.
13. Hille B (2001) *Ion Channels of Excitable Membranes* (Sinauer, Sunderland, MA), 3rd Ed.
14. Kleinschmidt JH, Tamm LK (2002) Structural transitions in short-chain lipid assemblies studied by (31)P-NMR spectroscopy. *Biophys J* 83(2):994–1003.
15. Marsh D (2013) *Handbook of Lipid Bilayers* (CRC Press, Boca Raton, FL), 2nd Ed.
16. Kaufmann K, Hanke W, Corcia A (1989) Ion channel fluctuations in pure lipid bilayer membranes: Control by voltage. Available at http://membranes.nbi.dk/Kaufmann/publications.html. Accessed January 10, 2013.
17. Antonov VF, Smirnova EYu, Shevchenko EV (1990) Electric field increases the phase transition temperature in the bilayer membrane of phosphatidic acid. *Chem Phys Lipids* 52(3-4):251–257.
18. Wodzinska K, Blicher A, Heimburg T (2009) The thermodynamics of lipid ion channel formation in the absence and presence of anesthetics. BLM experiments and simulations. *Soft Matter* 5:3319–3330.
19. Gu L-Q, Braha O, Conlan S, Cheley S, Bayley H (1999) Stochastic sensing of organic analytes by a pore-forming protein containing a molecular adapter. *Nature* 398(6729): 686–690.
20. Gu L-Q, Cheley S, Bayley H (2001) Capture of a single molecule in a nanocavity. *Science* 291(5504):636–640.
21. Banerjee A, et al. (2010) Molecular bases of cyclodextrin adapter interactions with engineered protein nanopores. *Proc Natl Acad Sci USA* 107(18):8165–8170.
22. Li W-W, et al. (2011) Tuning the cavity of cyclodextrins: Altered sugar adaptors in protein pores. *J Am Chem Soc* 133(6):1987–2001.
23. Monticelli L, et al. (2008) The MARTINI coarse grained force field: Extension to proteins. *J Chem Theory Comput* 4:819–834.
24. Bayley H, et al. (2008) Droplet interface bilayers. *Mol Biosyst* 4(12):1191–1208.
25. Hwang WL, Chen M, Cronin B, Holden MA, Bayley H (2008) Asymmetric droplet interface bilayers. *J Am Chem Soc* 130(18):5878–5879.
26. Heimburg T (2010) Lipid ion channels. *Biophys Chem* 150(1-3):2–22.
27. Mosgaard LD, Heimburg T (2013) Lipid ion channels and the role of proteins. *Acc Chem Res* 46(12):2966–2976.
28. Tieleman DP (2004) The molecular basis of electroporation. *BMC Biochem* 5:10.
29. Leontiadou H, Mark AE, Marrink SJ (2007) Ion transport across transmembrane pores. *Biophys J* 92(12):4209–4215.
30. Böckmann RA, de Groot BL, Kakorin S, Neumann E, Grubmüller H (2008) Kinetics, statistics, and energetics of lipid membrane electroporation studied by molecular dynamics simulations. *Biophys J* 95(4):1837–1850.
31. Antonov VF, Petrov VV, Molnar AA, Predvoditelev DA, Ivanov AS (1980) The appearance of single-ion channels in unmodified lipid bilayer membranes at the phase transition temperature. *Nature* 283(5747):585–586.
32. Lee AG (2003) Lipid-protein interactions in biological membranes: A structural perspective. *Biochim Biophys Acta* 1612(1):1–40.
33. Holt A, Killian JA (2010) Orientation and dynamics of transmembrane peptides: The power of simple models. *Eur Biophys J* 39(4):609–621.
34. Marsh D (2008) Protein modulation of lipids, and vice-versa, in membranes. *Biochim Biophys Acta* 1778(7-8):1545–1575.
35. Walker BJ, Krishnasastry M, Zorn L, Bayley H (1992) Assembly of the oligomeric membrane pore formed by staphylococcal alpha-hemolysin examined by truncation mutagenesis. *J Biol Chem* 267(30):21782–21786.
36. Walker B, Braha O, Cheley S, Bayley H (1995) An intermediate in the assembly of a pore-forming protein trapped with a genetically-engineered switch. *Chem Biol* 2(2):99–105.
37. Bayley H, Jayasinghe L, Wallace M (2005) Prepore for a breakthrough. *Nat Struct Mol Biol* 12(5):385–386.
38. Bayley H (2009) Membrane-protein structure: Piercing insights. *Nature* 459(7247): 651–652.
39. Mechaly AE, et al. (2011) Structural insights into the oligomerization and architecture of eukaryotic membrane pore-forming toxins. *Structure* 19(2):181–191.
40. Qian S, Wang W, Yang L, Huang HW (2008) Structure of transmembrane pore induced by Bax-derived peptide: Evidence for lipidic pores. *Proc Natl Acad Sci USA* 105(45):17379–17383.
41. Tait SW, Green DR (2010) Mitochondria and cell death: Outer membrane permeabilization and beyond. *Nat Rev Mol Cell Biol* 11(9):621–632.
42. Sobko AA, Kotova EA, Antonenko YN, Zakharov SD, Cramer WA (2006) Lipid dependence of the channel properties of a colicin E1-lipid toroidal pore. *J Biol Chem* 281(20):14408–14416.

43. Wendell D, et al. (2009) Translocation of double-stranded DNA through membrane-adapted phi29 motor protein nanopores. *Nat Nanotechnol* 4(11):765–772.
44. Wang HY, et al. (2013) Single-molecule DNA detection using a novel SP1 protein nanopore. *Chem Commun (Camb)* 49(17):1741–1743.
45. Rodriguez F, et al. (2013) Structural model for the protein-translocating element of the twin-arginine transport system. *Proc Natl Acad Sci USA* 110(12):E1092–E1101.
46. Wilke GA, Bubeck Wardenburg J (2010) Role of a disintegrin and metalloprotease 10 in staphylococcus aureus alpha-hemolysin-mediated cellular injury. *Proc Natl Acad Sci USA* 107(30):13473–13478.
47. Thompson JR, Cronin B, Bayley H, Wallace MI (2011) Rapid assembly of a multimeric membrane protein pore. *Biophys J* 101(11):2679–2683.
48. Kintzer AF, et al. (2010) Role of the protective antigen octamer in the molecular mechanism of anthrax lethal toxin stabilization in plasma. *J Mol Biol* 399(5):741–758.